continued convergence at a rate of 5 cm/year could have produced potential slip of 4 m. That amount of slip, if released today in one event, might generate a magnitude 8 earthquake in the remainder of the gap.

No specific premonitory phenomena are recognized at present in this region. McCann *et al.* (*3*) imply that the gap may be the site of a major earthquake within the next few years, based on the spatial-temporal pattern of earthquakes during the past 20 years. However, the timing could be affected by earthquakes in adjacent regions. For example, a major earthquake on the Denali-Totschunda-Chatham Strait fault system, which lies to the north and east, might partly relieve the stress within the gap, thus increasing the time until the next large earthquake. Nevertheless the region between Kayak Island and Icy Bay appears to be among the most likely sites for the next major earthquake in the United States. As such, the area should be the site of intensified observations, both for earthquake prediction and for studies of strong ground motion.

J. C. LAHR, C. D. STEPHENS
United States Geological Survey,
Menlo Park, California 94025
H. S. HASEGAWA
Earth Physics Branch, Department of
Energy, Mines and Resources,
Ottawa, Ontario, Canada K1A 0Y3
JOHN BOATWRIGHT
Lamont-Doherty Geological
Observatory of Columbia University,
Palisades, New York 10964

References and Notes

1. *U.S. Geol. Surv. Prelim. Determination Epicenters No. 7-79* (1979).
2. W. Thatcher and G. Plafker, *Int. Union Geod. Geophys. IASPEI/IAVCEI Assem. Abstr.* (1977), p. 54.
3. W. R. McCann, O. J. Pérez, L. R. Sykes, *Science* **207**, 1309 (1980).
4. D. G. Tobin and L. R. Sykes, *J. Geophys. Res.* **73**, 3821 (1968).
5. J. A. Kelleher, *ibid.* **75**, 5745 (1970); L. R. Sykes, *ibid.* **76**, 8021 (1971).
6. C. D. Stephens, J. C. Lahr, K. A. Fogleman, M. A. Allan, S. M. Helton, *U.S. Geol. Surv. Open-File Rep. 79-718* (1979).
7. J. C. Lahr, G. Plafker, C. D. Stephens, K. A. Fogleman, M. E. Blackford, *U.S. Geol. Surv. Open-File Rep. 79-670* (1979).
8. J. C. Lahr, thesis, Columbia University (1975).
9. J. B. Minster and T. H. Jordan, *J. Geophys. Res.* **83**, 5331 (1978).
10. H. Kanamori, *ibid.* **82**, 2981 (1977).
11. Y. B. Tsai and K. Aki, *ibid.* **75**, 5729 (1970); A. Ben-Menahem, *Bull. Seismol. Soc. Am.* **51**, 401 (1961).
12. G. Plafker and M. Rubin, *U.S. Geol. Surv. Open-File Rep. 78-943* (1978), p. 687.
13. T. R. Bruns and G. Plafker, *U.S. Geol. Surv. Open-File Map 75-508* (1975).

14. We thank R. A. Page and J. C. Savage for critically reading this report. This study was partly supported by the Outer Continental Shelf Environmental Assessment Program of the National Oceanic and Atmospheric Administration. This is Canadian Department of Energy, Mines and Resources Contribution 802.

18 June 1979; revised 8 November 1979

High-Pressure Phase in Americium Metal

Abstract. *X-ray diffraction studies at high pressure (above 150 kilobars) show that americium metal undergoes a phase change from a high-symmetry, face-centered cubic structure to an orthorhombic* α*-uranium structure. This transition results from the onset of* f*-electron bonding as the lattice is compressed.*

Studies on americium metal (*1*) have shown two stable structures at atmospheric pressure: a high-temperature, face-centered cubic (fcc) structure and a low-temperature (< 700°C) double hexagonal-close-packed (dhcp) phase. Stephens *et al.* (*2*) measured compressions to 30 kbar of samples containing both the fcc and dhcp forms. Akella *et al.* (*3*) reported an fcc structure at 65 kbar with a lattice constant of 4.684 Å. Our work extends compression values for americium metal to much higher pressures (~ 160 kbar) and reveals a third phase, the orthorhombic α-uranium structure. Since americium is the first actinide element to have nonbonding f electrons, this transition demonstrates that these f electrons can be forced to participate in the bonding under pressure.

Our sample contained 2000 parts per million (ppm) of ytterbium and less than 100 ppm of other impurities. Normally pure americium has the dhcp structure under ambient conditions. The presence of the ytterbium in our sample allowed the high-temperature fcc phase to be retained after quenching (*4*).

The experimental apparatus included a diamond anvil cell with a film cassette described by Bassett *et al.* (*5*). The diamonds had a culet diameter of 600 μm. A 265-μm-thick gasket (Inconel X-750) preindented to 60 μm was used with a hole diameter of 190 μm. The sample chamber formed by the hole in the gasket and the diamond tips contained the ytterbium-stabilized americium sample, several single-crystal ruby chips and powdered aluminum for the pressure calibration measurements, and silicone diffusion pump oil to serve as a quasi-hydrostatic pressure medium.

Pressures were measured by the ruby fluorescence method (*6*) before and after each film exposure (except for the measurements at 177 kbar). After pressure changes, the cell was allowed to relax for at least 1 day before any data were taken. For each pressure measurement, a ruby chip from the original supply was used as a temperature standard at 1 bar to eliminate errors due to possible temperature shifts in the fluorescence lines. The compression of the powdered aluminum seen in the high-pressure diffraction patterns provided a check on the sample-to-film distance. Independent pressure determinations from the ruby fluorescence and aluminum diffraction lines were in good agreement within their respective error limits.

All x-ray diffraction patterns were made with Mo Kα radiation (wavelength $\lambda = 0.7107$ Å) and were recorded on Kodak Industrex AA film. The x-ray tube was operated at 45 kV and 20 mA, and exposure times were 500 to 600 hours. After the films were developed, they were scanned and their density values digitized. In this form the data were then processed with an image enhancement computer program (*7*); an additional enlargement was made to simplify measurements of the 2θ diffraction angles.

Diffraction films were obtained at

Table 1. Structural data for americium metal at pressure.

Pressure (kbar)	Structure type	Lattice constants (Å)	Unit cell volume	Atomic volume
0	fcc	$a = 4.894$	117.15	29.29
65*	fcc	$a = 4.684$	102.77	25.69
152 ± 2	Orthorhombic α-uranium	$a = 3.063 \pm 0.004$ $b = 5.968 \pm 0.010$ $c = 5.169 \pm 0.008$ $y = 0.1025 \pm 0.0025$	94.49	23.62
161 ± 2	Orthorhombic α-uranium	$a = 3.060 \pm 0.005$ $b = 5.962 \pm 0.011$ $c = 5.155 \pm 0.008$ $y = 0.1025 \pm 0.0025$	94.04	23.51
177 ± 2	Orthorhombic α-uranium	$a = 3.046 \pm 0.004$ $b = 5.957 \pm 0.009$ $c = 5.148 \pm 0.007$ $y = 0.1025 \pm 0.0025$	93.41	23.35

*From Akella *et al.* (*3*).

0036-8075/80/0321-1353$00.50/0

Table 2. Observed (o) and calculated (c) crystal data for americium metal at 152 kbar.

$\sin^2\theta_o$	d_o	I_o	$\sin^2\theta_c$	d_c	I_c	$hk\ell$
0.0169	2.7317	40	0.0170	2.7229	51.2	110
0.0188	2.5928	100	0.0189	2.5850	100.0	021, 002
0.0215	2.4256	50	0.0218	2.4092	42.5	111
0.0359	1.8745	40	0.0359	1.8747	38.9	112
0.0502	1.5864	30	0.0501	1.5873	33.4	131
0.0537	1.5329	10	0.0539	1.5300	8.6	200
0.0570	1.4889	20	0.0567	1.4923	20.4	023, 040
0.0598	1.4533	10	0.0595	1.4562	10.7	113
0.0730	1.3148	30	0.0728	1.3167	31.3	221, 202
0.0751	1.2963	10	0.0756	1.2925	12.6	042, 004
0.0881	1.1973	10	0.0879	1.1985	14.4	133
0.0933	1.1635	$-(311_{Al})$	0.0926	1.1676	9.7	114
0.1016	1.1147	$-(222_{Al})$	0.1021	1.1120	6.5	150

pressures of 111, 125, 152, 161, and 177 kbar. The diffraction patterns at 111 and 125 kbar were complex, and an interpretation will require further work. The higher pressure patterns could be unambiguously interpreted as from an α-uranium type structure (*8*). Except for two weak lines at large 2θ values, there were no overlapping or interfering lines from either the gasket material or the aluminum powder.

The structure from 152 to 177 kbar is the α-uranium orthorhombic with space group *Cmcm* (No. 63) and four atoms per unit cell located in spatial position set 4(*c*): $\pm(0,y,1/4)$; $\pm(1/2,1/2+y,1/4)$ (*9*). The lattice constants at 152 kbar are listed in Table 1. The position parameter $y = 0.1025 \pm 0.0025$ was found by trial to give a good fit to the intensity data. Powder diffraction intensities for Mo Kα radiation were calculated with neutral form factors and the ANIFAC program (*10*). Corrections were made for the Lorentz polarization factor but not for absorption or thermal motion of the atoms.

In Table 2, we list the observed and calculated values of $\sin^2\theta$, the interplanar distances d, and the relative intensities I, for the $(hk\ell)$ reflections observed from the sample at 152 kbar. Agreement between calculated and observed values is very good. Our americium crystallographic data at 152, 161, and 177 kbar are presented in Table 1 along with earlier lower pressure results of other workers. The relative volume change V/V_0 as a function of pressure is illustrated in Fig. 1. The three independent sets of data are in close agreement; the fact that they can be connected by a smooth curve indicates that the volume changes at the phase boundaries are small.

The high-pressure α′ phase of cerium has also been found to have the α-uranium structure (*11*). Thus, americium is the third element in which a phase with the α-uranium structure has been discovered and the second in which this occurred with pressure. Because α-uranium, α′-cerium, and the new phase of americium have different valences, the stability of the α-uranium structure appears to be independent of the number of bonding electrons.

The change from a typically metallic crystal structure (fcc) to an exotic one of low symmetry can be predicted on the basis of an increasingly evident appearance of 5*f*-like charge in the vicinity of the atomic cell boundary with increasing pressure. Calculations for free atoms in the actinide series show that with increasing atomic number the density of the 5*f*-like charge cloud at a distance corresponding to the point midway between the atoms reaches a maximum for plutonium (atomic number $Z = 94$) and then drops rapidly. The maximum is caused by the steady radial contraction of the 5*f* orbitals with a concurrently increasing *f*-shell electron population. Exotic structures at atmospheric pressure are seen in uranium ($Z = 92$), neptunium ($Z = 93$), and plutonium for which this swelling is the largest. The absence of an exotic structure in americium ($Z = 95$) at 1-bar densities is consistent with the contraction of the 5*f* shell into the core. However, with increasing compression, a stage is reached in americium where the density of the 5*f*-like charge midway between atoms is comparable with that of plutonium at low densities where the exotic α-plutonium structure exists.

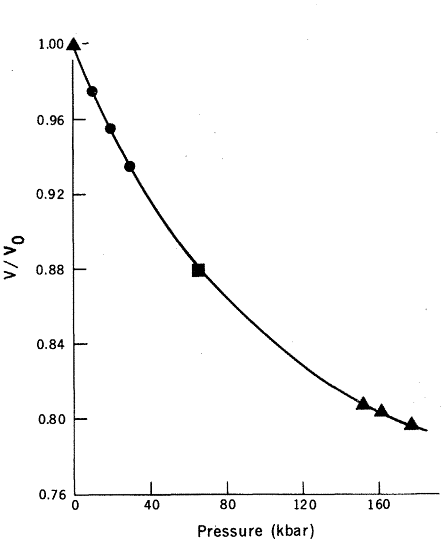

Fig. 1. Compression of americium metal: (●) representative points from Stephens *et al.* (*2*); (■) Akella *et al.* (*3*); and (▲) the present work.

On the basis of the radial charge densities calculated by means of a relativistic atomic structure program (*12*) for the americium atom, the corresponding density of the metal is predicted to be about 18 percent above normal, in agreement with our measurements. Therefore, by applying pressure we have compressed the atomic cell sufficiently to enable the normally unexposed *f* electrons to participate in the bonding as they do in plutonium at its normal density.

R. B. Roof
Los Alamos Scientific Laboratory,
Los Alamos, New Mexico 87545
R. G. Haire
Oak Ridge National Laboratory,
Oak Ridge, Tennessee 37830
D. Schiferl
L. A. Schwalbe
E. A. Kmetko
J. L. Smith
Los Alamos Scientific Laboratory

References and Notes

1. P. Graf, B. B. Cunningham, C. H. Dauben, J. C. Wallman, D. H. Templeton, H. Ruben, *J. Am. Chem. Soc.* **78**, 2340 (1956); D. B. McWhan, J. C. Wallman, B. B. Cunningham, L. B. Asprey, F. H. Ellinger, W. H. Zachariasen, *J. Inorg. Nucl. Chem.* **15**, 185 (1960); J. C. Spirlet and W. Mueller, *J. Less-Common Met.* **31**, 35 (1973).
2. D. R. Stephens, H. D. Stromberg, E. M. Lilley, *J. Phys. Chem. Solids* **29**, 815 (1968).
3. J. Akella, Q. Johnson, W. Thayer, R. N. Schock, *J. Less-Common Met.* **68**, 95 (1979).
4. J. L. Smith and R. G. Haire, *Science* **200**, 535 (1978); J. L. Smith, in *Proceedings of the Third Conference on Superconductivity in d- and f-Band Metals* (Academic Press, New York, in press).
5. W. A. Bassett, T. Takahashi, P. M. Stook, *Rev. Sci. Instrum.* **38**, 37 (1967).
6. R. A. Forman, G. J. Piermarini, J. D. Barnett, S. Block, *Science* **176**, 284 (1972); J. D. Barnett, S. Block, G. J. Piermarini, *Rev. Sci. Instrum.* **44**, 1 (1973); G. J. Piermarini, S. Block, J. D. Barnett, R. A. Forman, *J. Appl. Phys.* **46**, 2774 (1975); H. K. Mao, P. M. Bell, J. Shaner, D. Steinberg, *ibid.* **49**, 3276 (1978).
7. This work was performed by Group M-8, Los Alamos Scientific Laboratory (D. Janney, group leader). A two-dimensional digitizing microdensitometer extracts data from the diffraction film for computer enhancement. The enhancement algorithm estimates the noise of the film and determines whether each point is significantly different from the average value of its close neighbor points. Each data point is set to one of three levels (white, gray, or black), depending on whether it is significantly less than, equal to, or greater than its close neighbors. The diffraction pattern may make several sequential passes through the algorithm. Diffraction lines that are initially very faint may then display high contrast. Although position data are preserved, some intensity data are lost during the enhancement. A positional scale is synthesized in the

computer and added to the image as a measurement aid.
8. C. W. Jacob and B. E. Warren, *J. Am. Chem. Soc.* **59**, 2588 (1937); R. W. G. Wyckoff, *Crystal Structure* (Interscience, New York, ed. 2, 1963), vol. 2.
9. *International Tables for X-ray Crystallography* (Kynoch, Birmingham, England, 1952), vol. 1.
10. A. C. Larson, R. B. Roof, D. T. Cromer, "ANIFAC" (Report LA-3335, Los Alamos Scientific Laboratory, Los Alamos, N.M., 1965); *International Tables for X-ray Crystallography* (Kynoch, Birmingham, England, 1974), vol. 4.
11. W. H. Zachariasen and F. H. Ellinger, *Acta Crystallogr. Sect. A* **33**, 155 (1977); F. H. Ellinger and W. H. Zachariasen, *Phys. Rev. Lett.* **32**, 773 (1974).
12. D. Liberman, J. T. Waber, D. T. Cromer, *Phys. Rev.* **137**, A27 (1965).
13. We thank W. H. Zachariasen (who died on 24 December 1979) and R. N. R. Mulford for assistance and discussions. We also thank J. Akella, Q. Johnson, W. Thayer, and R. N. Schock for communicating some of their results prior to publication. Work was performed under the auspices of the Department of Energy.

1 November 1979; revised 26 December 1979

Oxygen in the Sea Bottom Measured with a Microelectrode

Abstract. *The depth of penetration of oxygen into coastal marine sediments (water depth, 4 to 44 meters; 6° to 10°C) varied from 1 to 5.5 millimeters, as measured with membrane-covered oxygen microelectrodes. Below these upper few millimeters, oxygen was present only in the immediate vicinity of animal burrows. The depth of oxygen penetration is related to the rate at which oxygen is consumed in the sediment.*

Although the oxygen supply of marine sediments is of great importance to the benthic community, such information has been virtually nonexistent. The main reason is that no satisfactory method has been available for the accurate detection of sedimentary pore water concentrations. Because better estimates are lacking, the thickness of the brown, oxidized surface sediment having a positive oxidation-reduction potential has often been used as an indication of the penetration depth of oxygen into sediments (*1*). With the aid of polarographic oxygen microelectrodes, we have made the first accurate measurements of oxygen in marine sediments and have demonstrated the absence of oxygen in the deeper parts of this layer (*2*). The anoxic part of the brown layer is often much thicker than the oxic part. Earlier estimates of the depth of oxygen penetration into sediments therefore tend to be too high. We found that it is possible to calculate the approximate depth of oxygen penetration from the rate of oxygen uptake by the sediment surface, and this parameter is normally measured in sediment studies.

All the sediment samples were collected during a 2-week period in late November 1978. The sampling localities, all in coastal Danish waters, were situated at water depths from 4 to 44 m. The sediment was sampled with a Haps corer (*3*), from which subsamples were taken out with Plexiglas cylinders (inside diameter, 46 mm). Only cores for which there was no resuspension of the sediment material during the sampling procedure were used in the analysis. Oxygen profiles and the oxygen consumption rate of the sediment were determined while the cores were protected from light, immediately after sampling. The oxygen profiles were measured with the oxygen microelectrode of Baumgärtl and Lübbers (*4*), which has a tip diameter of 2 to 8 μm and therefore creates almost no physical or chemical distortion when it is inserted into the sediment. [The use of oxygen microelectrodes in sediments is described in (*2*).] The electrodes were introduced stepwise into the sediment from above with the aid of a micromanipulator, and the oxygen concentrations read at 0.5- or 1.0-mm intervals. The water above the sediment was stirred and kept saturated with air by bubbling. The oxygen consumption per unit area was calculated from the rate of decrease in oxygen concentration of the water above the sediment, as measured in stoppered sediment cores. Mean values of five cores with gently stirred water and five cores with no stirring were used (*5*). The porosity of the sediment (ϕ) was determined as the weight loss of a known volume of surface sediment (0 to 1 cm) after drying at 105°C for 24 hours.

The oxygen concentration in the pore water, C_x, at depth x may be calculated from (*6*):

$$C_x = \frac{R}{2D}\left[x^2 - 2x\left(\frac{2DC_0}{R}\right)^{1/2} + \frac{2DC_0}{R}\right] \tag{1}$$

where R is the oxygen uptake rate per unit volume of pore water, D is the diffusion coefficient of oxygen in the sediment, and C_0 is the oxygen concentration at the sediment surface. Equation 1 is valid only if the rate of oxygen consump-

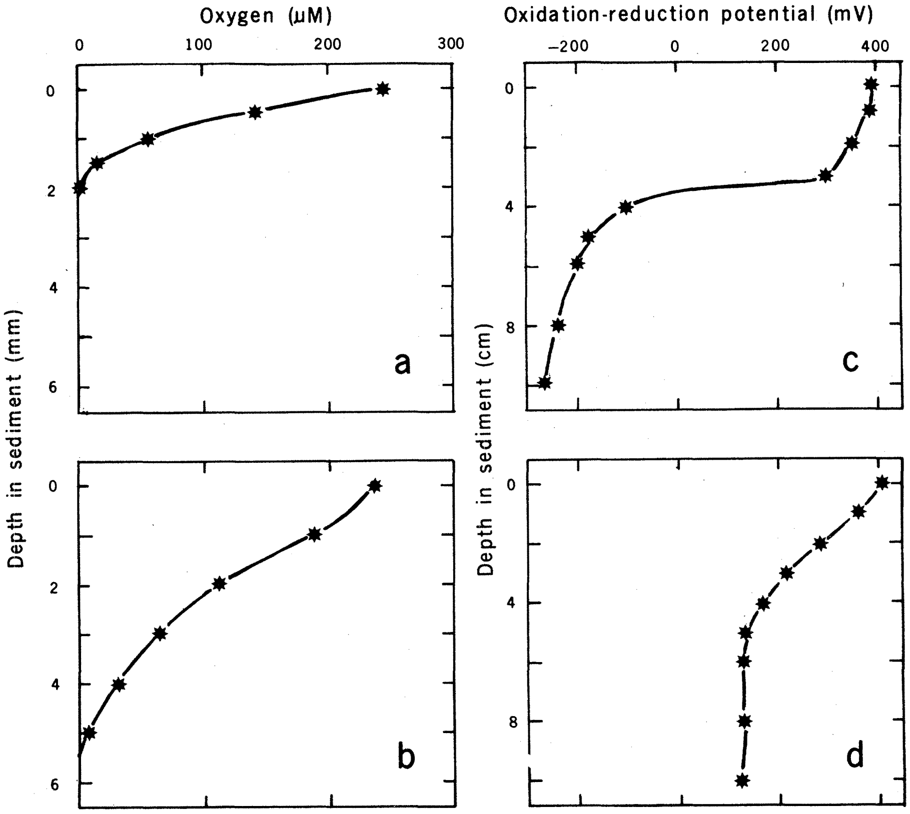

Fig. 1. Oxygen and oxidation-reduction profiles from two different sediments. (a) Oxygen profile showing the normal, nearly parabolic shape predicted by Eq. 1. (b) Sigmoidal oxygen profile, indicating turbulent oxygen transport in the upper 1 mm. (c) Oxidation-reduction profile from the same locality as (a). (d) Oxidation-reduction profile from the same locality as (b). A platinum electrode was used for the oxidation-reduction measurements (*15*). At both localities, the oxidized sediment layer having a positive oxidation-reduction potential was much thicker than the oxic layer.

0036-8075/80/0321-1355$00.50/0 Copyright © 1980 AAAS